Cerebral Cortex, September 2018;28: 3356–3371

doi: 10.1093/cercor/bhy144
Advance Access Publication Date: 28 June 2018
Original Article

ORIGINAL ARTICLE

An Autonomic Network: Synchrony Between Slow Rhythms of Pulse and Brain Resting State Is Associated with Personality and Emotions

Ehsan Shokri-Kojori[1], Dardo Tomasi[1] and Nora D. Volkow[1,2]

[1]Laboratory of Neuroimaging, National Institute on Alcohol Abuse and Alcoholism, National Institutes of Health, Bethesda, MD 20892, USA and [2]National Institute on Drug Abuse, National Institutes of Health, Bethesda, MD 20892, USA

Address correspondence to Ehsan Shokri-Kojori, Laboratory of Neuroimaging, National Institute on Alcohol Abuse and Alcoholism, National Institutes of Health, Bethesda, MD, USA. Email: ehsan.shokrikojori@nih.gov

Abstract

The sympathetic system's role in modulating vasculature and its influence on emotions and personality led us to test the hypothesis that interactions between brain resting-state networks (RSNs) and pulse amplitude (indexing sympathetic activity) would be associated with emotions and personality. In 203 participants, we characterized RSN spatiotemporal characteristics, and phase–amplitude associations of RSN fluctuations with pulse and respiratory recordings. We found that RSNs are spatially reproducible within participants and were temporally associated with low frequencies (LFs < 0.1 Hz) in physiological signals. LF fluctuations in pulse amplitude were not related to cardiac electrical activity and preceded LF fluctuations in RSNs, while LF respiratory amplitude fluctuations followed LF fluctuations in RSNs. LF phase dispersion (PD) (lack of synchrony) between RSNs and pulse (PD_{pulse}) (not respiratory) correlated with the common variability in measures of personality and emotions, with more synchrony being associated with more positive temperamental characteristics. Voxel-level PD_{pulse} mapping revealed an "autonomic brain network," including sensory cortices and dorsal attention stream, with significant interactions with peripheral signals. Here, we uncover associations between pulse signal amplitude (presumably of sympathetic origin) and brain resting state, suggesting that interactions between central and autonomic nervous systems are important for characterizing personality and emotions.

Key words: brain-body connection, interoception, personality–emotion *g* factor, photoplethysmography, fMRI

Introduction

What makes us unique as individuals is thought to be an emergent property of our distinct brains. Yet, since ancient times, there have been recognized associations between the brain and the body in the way they shape our behavior ("Mens sana in corpore sano"- Juvenal; Satire X, 120 CE). Most notable are the associations between cardiovascular function and emotions and personality (Pozuelo 2012). As such, types A and D personality traits have been considered as risk factors for cardiovascular disease (Jenkins et al. 1974; Denollet et al. 2006). Similarly, strong emotional events can trigger arrhythmias and heart failure, which mostly reflect the brain's role in regulating cardiac function through the autonomic nervous system (Wittstein et al. 2005; Wilbert-Lampen et al. 2008). However, there is also evidence that the cardiovascular system interacts

© The Author(s) 2018. Published by Oxford University Press.
This is an Open Access article distributed under the terms of the Creative Commons Attribution Non-Commercial License (http://creativecommons.org/licenses/by-nc/4.0/), which permits non-commercial re-use, distribution, and reproduction in any medium, provided the original work is properly cited. For commercial re-use, please contact journals.permissions@oup.com

with brain functions including emotions. The onset of atrial fibrillation has been shown to precede psychological distress and negative emotionality (McCABE et al. 2011), and heart-rate variability driven by self-paced breathing patterns has been linked to changes in perceived fear and anxiety (Nardi et al. 2006; Homma and Masaoka 2008).

A range of neuroimaging measures have been linked to positive and negative aspects of human personality and emotions, including brain dopamine activity (Depue et al. 1994), metabolic activity in orbitofrontal cortex (Volkow et al. 2011), asymmetry in the alpha-band of electroencephalography signals (De Pascalis et al. 2013), serotonin neurotransmission (Lesch et al. 2012), and regional differences in brain tissues (Mincic 2015). More importantly, there are indications suggesting interactions between the brain, cardiovascular system, and emotions (Fredrickson and Levenson 1998; Sadeghi et al. 2013). In this relation, pioneering experiments revealed an association between heartbeat detection performance (indexing interoceptive sensitivity) (Brener and Ring 2016) and intensity of perceived emotions (Katkin et al. 1981; Wiens et al. 2000). This association has been linked to the insula and cingulate cortex, which are involved in interoception (Critchley et al. 2004; Pollatos et al. 2005; Craig 2009). Recent research suggests an association between immediate heartbeat-evoked cortical activity and human perceptual capacity (Park et al. 2014). Although there are indications that features of cardiovascular and respiratory signals (e.g., rate variability) and brain resting fluctuations are associated (Chang and Glover 2009; Jennings et al. 2015; Nikolaou et al. 2016), many studies have attributed these associations to nonneuronal effects (Wise et al. 2004; Shmueli et al. 2007).

The recognized modulatory role of the cortex (e.g., insula or cingulum) (Marins et al. 2016) in the regulation of the autonomic system and the sensitivity of the cortex to physiological signals (Duschek et al. 2015) suggest bidirectionality in the interactions between the brain and autonomic system. For example, the associations between respiratory sinus arrhythmia and brain alpha activity have been considered a bottom-up modulation of the cortex (Duschek et al. 2015), while the temporal lag between activity in ventromedial prefrontal cortex and skin conductance signal has been considered a top-down cortical control of physiological regulation (Gabard-Durnam et al. 2014). From a theoretical perspective, the neurovisceral integration model (Thayer and Lane 2000, 2002) highlights the role of prefrontal–subcortical inhibitory circuits in both emotional self-regulation and cardiovascular function through the vagus nerve, which predominantly mediates peripheral parasympathetic signaling (Park and Thayer 2014). In contrast, the sympathetic system plays a primary role in the extrinsic innervation of the cerebral vasculature through perivascular nerves (Hamel 2006). The sympathetic system is constantly involved in maintaining homeostasis (Brodal 2004), for example, it prepares the body for action by constricting nonvital vessels while dilating vital (coronary and) cerebral arteries through perivascular nerves. The extrinsic innervation acts along with the intrinsic innervation of perivascular nerves which regulate cerebral blood flow through neuronal–astrocytic–vascular units (i.e., neurovascular coupling) (Hamel 2006; Peterson et al. 2011). When considering noninvasive measures of autonomic nervous system activity in MRI, low-frequency (LF < 0.1 Hz) variability in the blood volume pulse, as measured by amplitude of the photoplethysmography (PPG, also referred to as *pulse*) signal, has been suggested as an indicator of sympathetic (neurogenic) activity (Nitzan et al. 1996; Landsverk et al. 2007; Mizeva et al. 2015) that reflects the sympathetic regulation of vasomotor function (Wallin and Charkoudian 2007). Specifically, increases in sympathetic tone mediates vasoconstriction in arteries and veins (Klabunde 2011), limiting blood volume, and leading to decreases in pulse signal amplitude (and vice versa) (Gil et al. 2008). Therefore, changes in the sympathetic tone are expected to be correlated with changes in the pulse amplitude. This association has been documented previously (Awad et al. 2001; Millasseau et al. 2006; Allen 2007; Shelley 2007; Chan et al. 2010; Murphy et al. 2013).

Interestingly, characteristics of pulse signal amplitude have been associated with positive and negative emotional states (Xia et al. 2017) or arousal (Kim et al. 2010). Similarly, an association between pulse (combined with other physiological measures) and personality traits and arousability has been also reported (Suls et al. 1998). Moreover, there is evidence that LF fluctuations in brain activity may in part have a sympathetic origin (Taylor et al. 2015; Triggiani et al. 2016). The (extrinsic) effects of sympathetic activity on cerebral blood flow (Harper et al. 1972; Hamel 2006) and the known associations between the sympathetic system and emotions (Kreibig 2010; Kop et al. 2011) and personality (LeBlanc et al. 2004; Lester 2012) motivated our core hypothesis that vascular signaling (likely mediated by sympathetic tone) contributes to activity in the cortex (Park et al. 2014; Winston and Rees 2014) and that cortex sensitivity to vascular signaling would be associated with an aspect of emotions and personality. Thus, we predicted that LF pulse amplitude fluctuations would precede those in the brain resting-state signal fluctuations. Individual differences in the sensitivity of cortex to vascular signaling could be related to differences in vascular-induced neuronal activity (Moore and Cao 2008; Zhang and Liao 2015) that may reflect differences in mechanoreceptor density in the cortex (Zimny et al. 1986). We characterized the sensitivity of cortex to vascular signaling using an index of synchrony between pulse amplitude fluctuations and resting-state fMRI signal. Based on evidence suggesting associations between interoceptive abilities and emotion processing (Wiens et al. 2000; Gray et al. 2012; Pfeifer et al. 2017), and that lower heartbeat-evoked potentials were associated with worse emotional outcomes and personality disorders (Müller et al. 2015), we predicted that higher temporal synchrony in the amplitude fluctuations of pulse and brain resting-state networks (RSNs) would be related to more positive ratings on emotions and personality traits. For this purpose, we studied the first principal components (PCs) of personality and emotion categories, capturing common variability in these categories, for the associations with the brain imaging measures (see Behavioral Assessments).

It is worth noting that our approach is in contrast to prior studies that focused on the association between cardiac-rate variability (Shmueli et al. 2007; Jennings et al. 2015; Nikolaou et al. 2016) or respiratory-rate variability (Chang and Glover 2009) and the fMRI signal. Though sympathetic activity also affects heart rate, the associations between low-frequency pulse amplitude fluctuations and low-frequency heart-rate variability are not consistent across individuals (Nitzan et al. 1996). LF heart-rate variability is influenced by both sympathetic and parasympathetic activity (Stauss 2003) and it is not a reliable measure of sympathetic activity alone (Houle and Billman 1999; Monfredi et al. 2014). Thus, we did not use low-frequency heart-rate variability as a primary index of sympathetic tone. Yet, we tested associations between brain RSNs and pulse-rate (or respiratory-rate) variability. We also performed a separate experiment ($n = 6$) to rule out that LF fluctuations in the pulse amplitude are related to cardiac electrical activity.

Methods

Participants

Out of 511 participants from Q1–Q6 data releases of the Human Connectome Project (HCP, http://www.humanconnectome.org/), 203 participants were included in this study (see Supplementary Table S1 for participant IDs and summaries of drug/alcohol measures). For our study, the following exclusion criteria were considered: incomplete resting-state fMRI sessions, incomplete physiological recordings (see Section Physiological Monitoring), or excessive motion (see Section MRI Processing). For HCP inclusion criteria (e.g., age: 22–35 or no significant history of psychiatric disorder) and exclusion criteria (e.g., genetic disorders or history of head trauma) see Van Essen et al. (2012). All participants provided written informed consent according to the scanning protocol approved by Washington University in the St. Louis's Human Research Protection Office (HRPO), IRB# 201 204 036. No experimental activity with any involvement of human subjects took place at the author's institutions. Mean (±SD) participant age was 29.09 (±3.59); 124 of whom were females.

In a second cohort (n = 6, 6 females), with mean age (±SD) = 33.33 (±9.46), we collected physiological data (cardiac and pulse signals) at the National Institutes of Health (NIH). Participants were older than 18 years and could provide written informed consent, as approved by the institutional review board at the NIH. Exclusion criteria included past or current DSM-IV or DSM-5 diagnosis of a psychiatric disorder, history of head trauma, use of psychoactive medications 2 weeks prior to the study, body weight over 250 kg, and a positive test for drugs and/or pregnancy (for females) at the time of study.

Behavioral Assessments

HCP data included standardized behavioral assessments on a range of tasks from which we included personality and emotion categories (as well as alertness, cognition, motor, and sensory categories). The personality category included the 5-factor model instrument, indexing agreeableness, openness, conscientiousness, neuroticism, and extroversion (Costa and McCrae 1992). The emotion category included 5 instruments including emotion recognition (5 scores from Penn Emotion Recognition Test), and self-reports of negative affect (including anger-affect, anger-hostility, anger-aggression, fear-affect, fear-somatic, and sadness surveys), psychological well-being (including life satisfaction, meaning and purpose, and positive affect surveys), social relationships (including friendship, loneliness, perceived hostility, perceived rejection, emotional support, and instrumental support surveys), and stress (including perceived stress and self-efficacy surveys) from the NIH Toolbox (Gershon et al. 2010). To reduce data dimension, for each category, the first PC of the variance normalized scores (age unadjusted) of the instrument tasks were computed. Supplementary Tables S2 and S3 summarize the test scores for each category and the extent to which they contributed to their corresponding PC. Personality PC accounted for 41.60% of the variance in personality tasks whereas the emotion PC accounted for 32.89% of emotion tasks (see Supplementary Fig. S1). Both PCs were positively loaded on negative traits (Supplementary Tables S2 and S3).

Scanning Protocol

HCP MRI data were acquired using a 32-channel coil with a 3.0 T Siemens Skyra scanner according to procedures approved by the IRB at Washington University (Van Essen et al. 2012, 2013). Resting-state functional images were acquired while participants relaxed in a darkened room with eyes open while they viewed a fixation cross-hair projected on a dark background. Data acquisition included a gradient-echo-planar imaging (EPI) sequence with multiband factor 8, repetition time (TR) 720 ms, echo time 33.1 ms, flip angle 52°, 104 × 90 matrix size, 72 slices, 2-mm isotropic voxels, and 1200 time points collected in 14:33 min. Resting-state scans were acquired in 4 runs on 2 separate days (REST1 and REST2). In each day, 2 resting-state runs were collected using different phase-encoding directions: left-to-right and right-to-left.

Physiological Monitoring

HCP data included pulse (photoplethysmography; PPG) and respiratory recordings that were acquired at 400 samples per second using Siemens pulse oximeter and respiratory belt. The data were linked to the onset of fMRI volume acquisition using the trigger signal from the MRI acquisition sequence. The spectral content of the pulse and respiratory signals was individually inspected and subjects with corrupt or partial physiological data in any of the 4 fMRI runs were not included in this study (see Supplementary Fig. S7). In the second cohort (n = 6), we collected PPG from the index finger in left and right hands as well as ECG (with 3 leads) with 1000 Hz sampling rate using BIOPAC (BIOPAC Systems Inc., Goleta, CA, USA). The recordings were continued for about 7 min and data for each participant were truncated into a 6-min segment (with minimal distortion and motion artifacts).

Physiological Signal Processing

After data acquisition, pulse and respiratory signals were down-sampled using an average of the signals along the instances where the trigger signal was high (i.e., active acquisition). The physiological signal acquisition was only active for 1188 TRs (from a total of 1200 TRs) relative to the onset of each resting-state run, resulting in 1188 down-sampled time points (TR = 0.72 s) for pulse and respiratory signals. We also estimated pulse-rate variability and respiratory-rate variability (see Supplementary Fig. S3*b*). While physical activity and some mental stressors may affect the agreement between pulse rate variability and heart rate variability (Schäfer and Vagedes 2013), pulse rate variability is considered a sufficiently accurate estimate of heart rate variability at rest (Schäfer and Vagedes 2013) in healthy individuals (Bolanos and Nazeran 2016). For this purpose, prior to down-sampling, the extracted pulse and respiratory (amplitude) time courses underwent an automated peak detection approach using the "findpeak" function in MATLAB (MathWorks, Inc., Natick, MA, USA). To ensure accuracy of peak detection, the minimum peak prominence was set to half of the signal standard deviation, and the minimum peak distance was set to 0.375 s for pulse peaks and to 2 s for respiratory peaks. Next, the inverse of the time difference between peak locations was assigned to the time points after a peak (and before next peak) as the rate measure for that interval. Finally, the rate data were down-sampled relative to the onset of fMRI trigger signal. For the second cohort, physiological data were processed in MATALB for down-sampling (TR = 0.385 s).

MRI Processing

Preprocessing was performed using the minimal processing pipeline for HCP data (Glasser et al. 2013). For each run, we used 2 available versions of resting fMRI data; the "raw" resting-state scans which underwent gradient distortion correction, rigid body realignment, EPI image distortion correction, spatial normalization to the stereotactic space of the Montreal Neurological

Institute (MNI), and brain masking (2-mm isotropic); and the "clean" datasets which in addition to the prior steps performed on the "raw" data underwent high-pass filtering (cutoff = 1/2000 Hz) (Smith et al. 2013) and independent component analysis (ICA)-based denoising (Salimi-Khorshidi et al. 2014). In brief, the ICA-based denoising identifies components in the data using a hierarchical classifier, in 3 main categories: "signal," "noise," and "unknown." The "noise" components represented motion, white matter signal, interaction of susceptibility artifacts and head motion, cardiac pulsation/arterial contribution, effects of large veins, or MRI acquisition-related noise (Salimi-Khorshidi et al. 2014). The identified noise components were removed from the data. All included participants had less than 0.5 mm mean frame-wise displacement (Power et al. 2012) in all 4 resting-state runs.

Independent Component Analysis

ICA is an effective approach for reducing the dimensionality of resting-state data into a few major networks in the subject space (Beckmann et al. 2005). Spatial ICA (a variant of ICA for when there are fewer time points than brain voxels) (Calhoun et al. 2001) was performed by running the "melodic" function (Beckmann and Smith 2004) in the University of Oxford's Center for Functional Magnetic Resonance Imaging of the Brain (FMRIB) Software Library (FSL) release 5.0 (http://www.fmrib.ox.ac.uk/fsl), on both raw and clean datasets for each run and each subject. Next, an automated component identification approach was used to extract spatial maps and time courses of 7 major cortical networks that are commonly found in task and resting-state conditions (Smith et al. 2009), which included: medial visual (MVN), sensorimotor (SMN), and auditory (ADN) for sensory-related networks, and default mode (DMN), executive control (ECN), right frontoparietal (RFPN), and left frontoparietal (LFPN) for higher order networks. Specifically, Pearson's product-moment correlation between each network mask (Smith et al. 2009) and spatial maps of ICA components ("melodic_IC.nii") was computed in MATLAB. An ICA component with the highest spatial correlation with a given network mask was selected as the component representing a specific network. For the identified networks, the time series of activity was extracted (from "melodic" output files) and 1188 time points were extracted that matched the duration of physiological recordings. Finally, a fast Fourier transform was applied to compute the frequency spectra of variance-normalized RSN time courses.

Within-Subject Reproducibility

Intraclass correlation coefficient (ICC), a measure of test–retest reliability, was used to index absolute agreement (here referred to as reproducibility) (Hopkins 2000) between repeated measures of spatial features (e.g., the ICA z-score of a voxel for an RSN) or temporal features (e.g., the amplitude of RSN frequency bins) over different fMRI runs within subjects. Under an analysis of variance framework, we used a 2-way mixed model, ICC (3, 1), to model within-subject variability relative to between-subject variability with fixed levels of measurements (i.e., 2 phase-encoding directions in 2 sessions; $k = 4$) and $n = 203$ subjects (McGraw and Wong 1996):

$$\mathrm{ICC}(3,1) = \frac{\mathrm{MSR} - \mathrm{MSE}}{\mathrm{MSR} + (k-1)\mathrm{MSE} + k(\mathrm{MSC} - \mathrm{MSE})/n}.$$

where, MSR is the mean square for rows (subjects), MSE is the mean squared error, and MSC is the mean squares for columns (measurements). An ICC = 0 indicates no agreement between the measurements and ICC = 1 indicates complete agreement between the measurements. Generally, the magnitude of ICC values we obtained here did not indicate high test–retest reliability. Instead, we used statistical significance of ICC values (Termenon et al. 2016) to gauge within-subject reproducibility of spatiotemporal indices using an F-test (McGraw and Wong 1996):

$$F(df_1, df_2) = \frac{\mathrm{MSR}}{\mathrm{MSE}}$$
$$df_1 = n - 1$$
$$df_2 = (n-1) \times (k-1)$$

ICC was run in MATLAB using the ICC toolbox (http://www.mathworks.com/matlabcentral/fileexchange/22099-intraclass-correlation-coefficient–icc-).

Amplitude and Phase Associations Between Physiology and RSNs

Magnitude squared coherence analysis (Kay 1988) was performed with Welch's overlapped averaged periodogram method (Welch 1967) to assess the extent to which the amplitude of MRI signal fluctuations and those in physiology (i.e., pulse or respiratory amplitude fluctuations) correspond to each other at each frequency. Specifically, for the magnitude squared coherence between x and y, $C_{xy}(f)$, we have:

$$C_{xy}(f) = \frac{|P_{xy}(f)|^2}{P_{xx}(f)P_{yy}(f)},$$

where $P_{xy}(f)$ is the cross power spectral density (CPSD) of x and y and $P_{xx}(f)$ and $P_{yy}(f)$ are power spectral densities of x and y, respectively. Magnitude squared coherence was computed with 256 frequency bins (within 0–0.69 Hz) using periodic Hamming windows with 50% overlap. For phase lag between x and y, the phase of the cross power spectral density of x and y was computed (Oppenheim and Schafer 2009). Specifically, CPSD per unit of frequency is defined as:

$$P_{xy}(f) = \sum_{m=-\infty}^{\infty} R_{xy}(m) e^{-i(2\pi f)m},$$

where $R_{xy}(m)$ is the cross-correlation function equal to:

$$R_{xy}(m) = E\{x_{n+m} y_n^*\},$$

where $E\{.\}$ represents the expected value operator, m represents time lag, and n is an implicit index. CPSD was computed with 256 frequency bins using periodic Hamming windows with 50% overlap. The CPSD yields a complex number for each frequency. The phase lag for each frequency bin was computed as the 4-quadrant inverse tangent of real over imaginary parts of CPSD:

$$\theta_{xy}(f) = \tan^{-1}\left(\frac{\mathrm{Re}(P_{xy}(f))}{\mathrm{Im}(P_{xy}(f))}\right).$$

All the analyses were performed in MATLAB using the Signal Processing toolbox

Phase Dispersion

Phase dispersion (PD) was defined to index the extent to which 2 signals deviate from being "phase-locked" and was computed

as the standard deviation of the phase lag between x and y within a given frequency range:

$$PD = \sqrt{\frac{1}{N-1}\sum_{i=J}^{K}(\theta_{xy}(f_i) - \hat{\theta}_{xy})^2},$$

where N is the number of frequency bins and f_i is the i-th frequency bin within the given frequency range (for 0.01–0.09 Hz: $J = 5$ to $K = 35$, a total of 31 bins) and $\hat{\theta}_{xy}$ is the average phase lag between x and y within the given frequency range. PD index is low if the 2 signals show temporal consistency or synchrony. The PD index was calculated for RSNs relative to pulse (PD_{pulse}) and relative to respiratory (PD_{resp}) fluctuations.

Results

To test our hypothesis, we first characterized spatial (brain regions) and temporal (frequency amplitudes) features of 7 major cortical RSNs (see Section Methods) (Smith et al. 2009). Next, we computed phase and amplitude of coherence between RSN signals and physiological recordings along the available RSN spectra (<0.7 Hz) and studied the effects of ICA-based cleaning on these associations to identify relevant frequency ranges in fMRI signal that are associated with physiological recordings after the cleaning step. Finally, we quantified the temporal consistency (i.e., synchrony) between RSNs and each physiological modality (i.e., respiratory and pulse recordings) and tested the extent to which this synchrony was related to human personality and emotions.

Spatiotemporal Characteristics of RSNs

There was significant spatial reproducibility for the regions that are known to be associated with each RSN ($p < 0.05$, Bonferroni; Fig. 1, Supplementary Fig. S2; Supplementary Tables S4–S10). Significant reproducibility was also observed in regions that were strongly anticorrelated with RSNs' time course (e.g., areas within the inferior occipital gyrus in the MVN) (Fig. 1, Supplementary Fig. S2, Supplementary Tables S4–S10). For temporal characteristics of RSNs, most of the spectral power (~90%) was concentrated below 0.1 Hz (Supplementary Table S11). Analysis of frequency amplitudes of raw and clean data (Fig. 1, Supplementary Fig. S2) suggested 3 distinct frequency ranges in the fMRI signal: LF range (LFR): 0–0.1 Hz, mid-frequency range (MFR): 0.1–0.2 Hz, and high-frequency range (HFR): 0.2–0.7 Hz. In all RSNs, LFR frequency amplitudes were not significantly reproducible. Across the MFR and HFR, the reproducibility of the RSN frequency amplitudes was highly significant for the raw data ($p < 0.05$, Bonferroni; Supplementary Table S12). But after ICA-denoising (which removes components from the data with characteristics of physiological signals, see Section Methods), the reproducibility of the frequency amplitudes in the higher order RSNs was no longer significant. In contrast, in the sensory RSNs, there was a reproducible frequency band primarily within the MFR that remained significant after ICA-denoising ($p < 0.05$, Bonferroni; Supplementary Table S12).

Amplitude of Coherence Between RSNs and Physiology

While the spectral average of pulse and respiratory amplitude fluctuations show that both signals have content under 0.1 Hz (Supplementary Fig. S3*a*), the pulse fluctuations showed a distinct peak at 0.07 Hz along with peaks at the main respiratory (0.3 Hz) and pulse (1.14 Hz) frequency components. For the amplitude of coherence between RSNs and pulse fluctuations and between RSNs and respiratory amplitude fluctuations, we found that the LFR and HFR (and marginally for MFR) in raw time courses of sensory RSNs had significant within-subject reproducibility (Figs 2 and 3; Supplementary Figs S4 and S5). This reproducibility of the coherence amplitude in the raw data was limited to HFR in higher order RSNs except for a small segment in LFR for ECN (Figs 2 and 3, Supplementary Figs S4 and S5). Consistent with HRF being within nominal respiratory frequencies, after ICA-denoising, the reproducibility of the coherence amplitude in HFR was no longer significant for any of the networks (Supplementary Tables S13 and S14). For LFR, the reproducibility of the coherence amplitude between physiology and sensory RSNs remained significant after ICA-denoising.

Cardiac-Pulse Associations

To better elucidate the nature of LFR pulse amplitude fluctuations, we performed coherence analyses between pulse signal in the left- and right-hand index fingers and between pulse signal and electrocardiogram (ECG) signal (indexing cardiac electrical activity) in LFR (Supplementary Fig. S6). While pulse signal between both hands showed a significant association in LFR ($t(5) = 3.96$, $p = 0.01$), association between pulse signal and ECG signal was not significant in LFR ($t(5) = 0.60$, $p = 0.58$).

Phase of Coherence Between RSNs and Physiology

The phase lag between RSNs' time course and respiratory and pulse signals revealed a distinct temporal order in the interaction between RSNs and physiological signals. The positive phase lag between pulse signal and all RSNs fluctuations in the LFR indicated that the slow-rate fluctuations in the pulse signal preceded those in RSNs (Fig. 2, Supplementary Fig. S4). This association was significantly reproducible in all sensory RSNs for raw data and for MVN and SMN in clean datasets, but not in higher order RSNs (Supplementary Table S15). For respiratory amplitude fluctuations, there was a negative lag between all RSNs and respiration in the LFR, indicating that respiratory amplitude fluctuations follow those in RSNs (Fig. 3, Supplementary Fig. S5). However, reproducibility of these phase associations was not significant for any of the RSNs. Phase associations between physiology and RSNs were overall insensitive to ICA-based denoising. For each subject, we computed the average phase lag across 4 runs in the LFR between physiology and cleaned RSN time courses, particularly between 0.01–0.09 Hz, a frequency range that shows reproducibility for phase and amplitude associations with physiology (Supplementary Tables S13–S15). All RSNs showed significant positive phase lags relative to pulse fluctuations (one sample t-test, $p < 0.0001$, 2-tailed; across all RSNs: $M_{phase} = 1.21$ rad, $SD_{phase} = 1.71$ rad), whereas all RSNs showed significant negative phase lags relative to respiratory amplitude fluctuations (one sample t-test, $p < 0.0001$, 2-tailed; across all RSNs: $M_{phase} = -1.59$ rad, $SD_{phase} = 1.07$ rad). Despite the apparent overlap in RSNs phase lags (Fig. 4*a*, *c*), the average phase lags differed between the RSNs relative to PPG (or pulse) amplitude fluctuations (main effect of RSN: $F(4.04, 816.47) = 16.79$, $p < 0.0001$) and between the RSNs relative to the respiratory amplitude fluctuations (main effect of RSN: $F(5.19, 1049.11) = 42.46$, $p < 0.0001$). The findings suggest that with respect to phase lag in LFR, RSNs might be differently associated with pulse and respiratory signals (Fig. 4). We also mapped the phase lag relative to pulse (Fig. 4*b*) and respiratory (Fig. 4*d*) fluctuations at the voxel

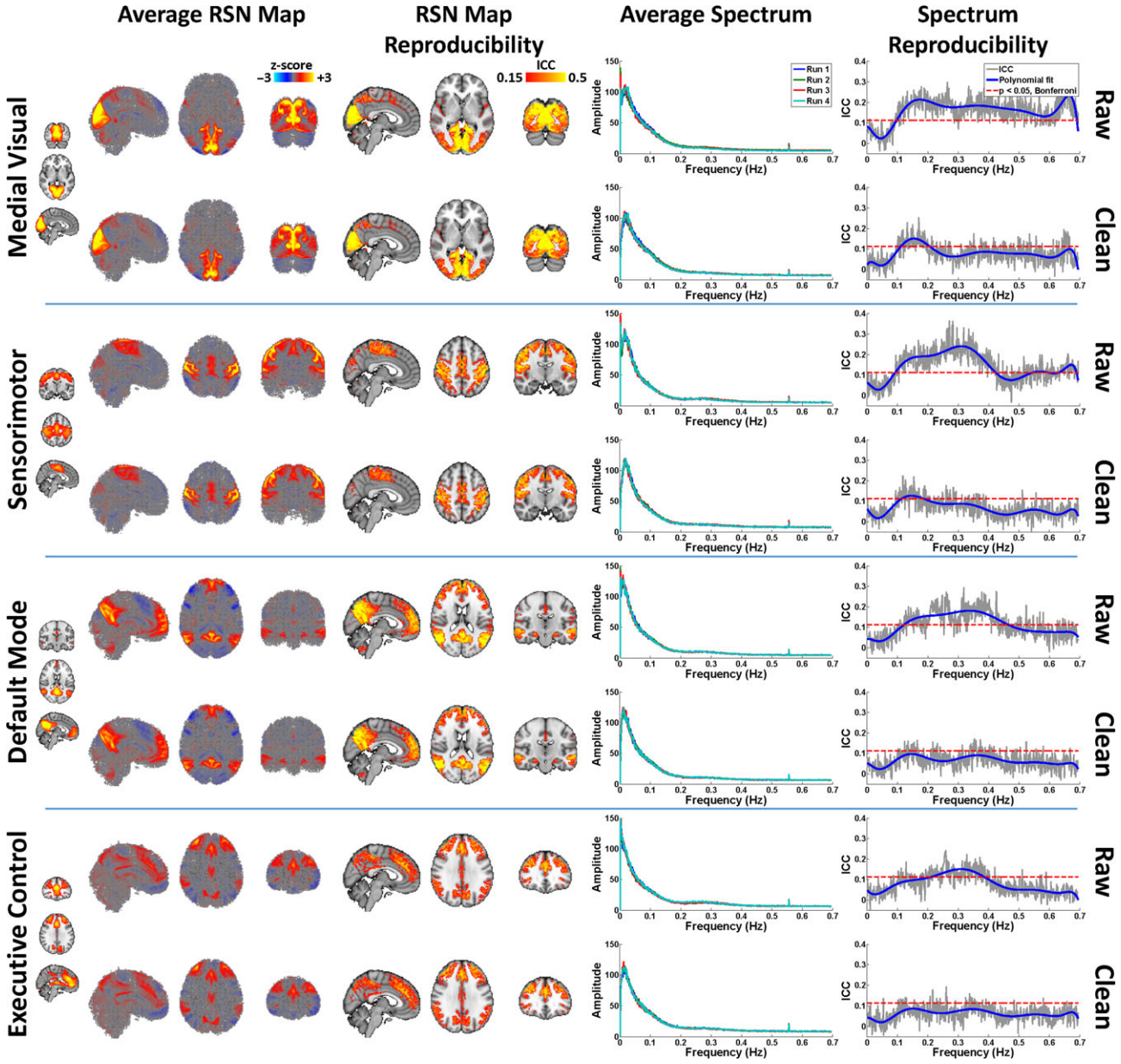

Figure 1. Spatiotemporal characteristics of RSNs. For each of MVN, SMN, DMN, and ECN, the spatial distribution of regions with highest association with each network (indexed by spatial ICA component z-scores) is shown under the first column for the average of 203 subjects (with no underlay image). For each RSN, the associations were similar for raw (top row) and clean (bottom row) datasets. The within-subject reproducibility of these spatial maps was assessed across the 4 fMRI runs using ICC(3, 1) for raw and clean datasets (with ICBM152 underlay image). The reproducibility maps are shown after thresholding ($p < 0.05$, Bonferroni). The spectral average of RSN time courses (594 bins) for each run is shown under the third column followed by the within-subject reproducibility of the amplitude of frequency bins of RSN fluctuations for raw and clean datasets (ICC(3, 1), $p < 0.05$, Bonferroni). Brain images are shown in radiological view.

level, which appeared to delineate main arterial pathways in the cerebral cortex. Finally, there was a positive phase between all RSNs and respiratory amplitude fluctuations in the HFR indicating respiration affects (precedes) RSN fluctuations at nominal respiratory rates (Fig. 3 and Supplementary Fig. S5).

PD of RSNs and Associations with Personality and Emotions

Finally, we characterized the extent to which synchrony in RSNs and pulse fluctuations is related to personality and emotions. We estimated the mean PD (0.01–0.09 Hz; see Section Methods) in the LFR of the 7 RSN networks (all showing a significant positive phase, Fig. 4*a*) relative to pulse amplitude fluctuations for each subject for each of 4 fMRI runs (Fig. 5*b*). An average of this index, which estimates the average of PD across the 7 RSNs and the 4 runs, was computed to represent PD_{pulse} for each subject (Fig. 5*a*). We found significant correlations between the first PC of personality measures (Supplementary Fig. S1*a*) and PD_{pulse} (Fig. 5*a*; $r(201) = 0.31$, $p < 0.00001$, 2-tailed), and between the first PC of emotion measures (Supplementary Fig. S1*b*) and PD_{pulse} (Fig. 5*c*; $r(201) = 0.23$, $p = 0.0012$, 2-tailed). These correlations were also significant within each of the 4 fMRI runs for personality PC (Fig. 5*b*, $p_1 = 0.045$, $p_2 = 0.005$, $p_3 =$

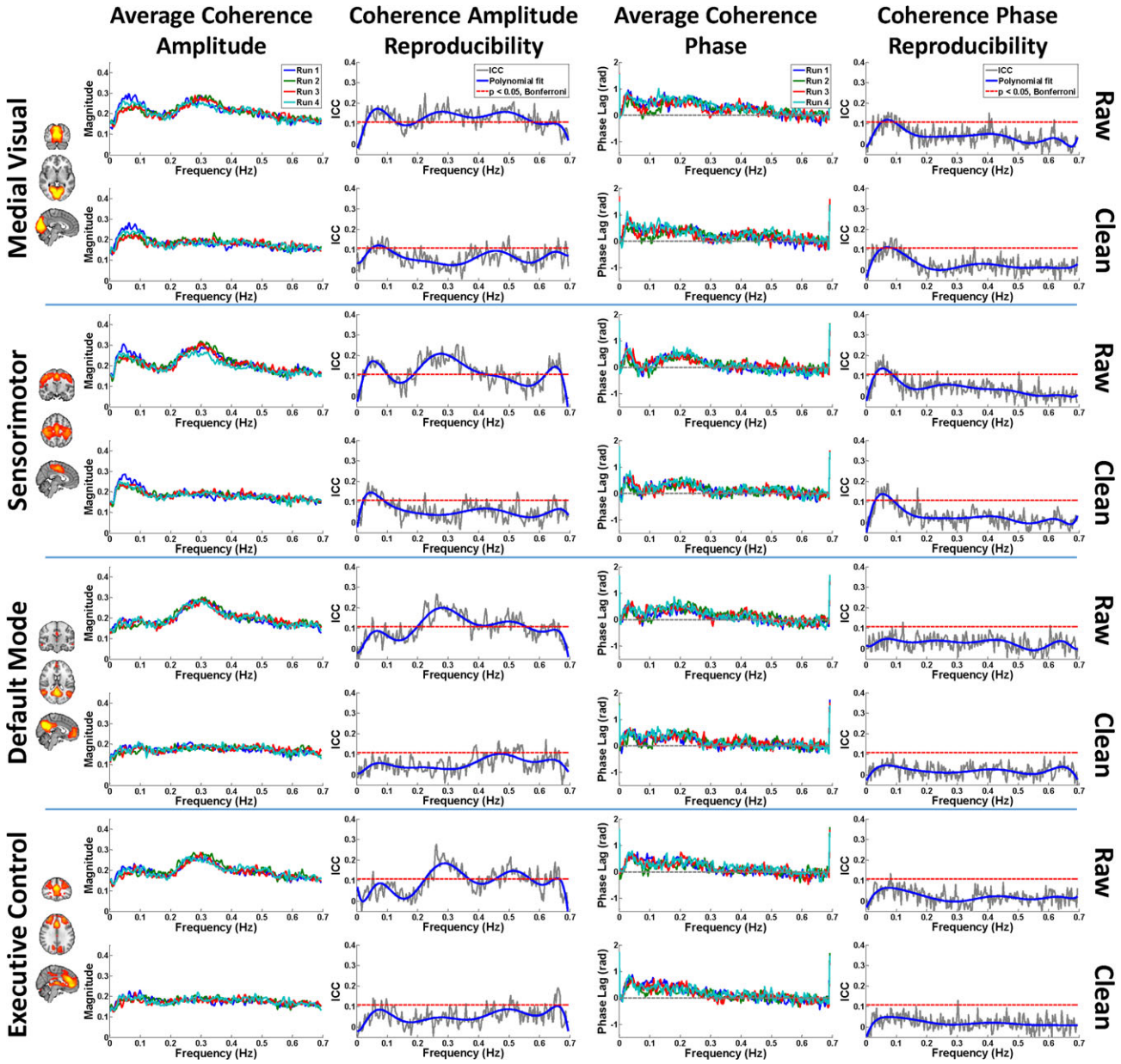

Figure 2. Amplitude and phase associations between RSNs and pulse amplitude fluctuations. First column shows the amplitude of coherence between RSNs and pulse signals for different frequency bins ($n = 256$), averaged across subjects for each fMRI run for raw (top row) and clean (bottom row) datasets. The within-subject reproducibility of these amplitude associations for each frequency bin was characterized using ICC(3, 1). The third column shows the coherence phase for each frequency bin averaged across subjects for each run, followed by the fourth column showing within-subject reproducibility of these phase measures for raw and clean datasets.

0.002, $p_4 = 0.0001$; 2-tailed) and were significant for 2 of the runs for emotion PC (Fig. 5*d*, $p_1 = 0.01$, $p_2 = 0.025$, $p_3 = 0.094$, $p_4 = 0.058$; 2-tailed). Higher PD_{pulse} (less temporal synchrony) was associated with negative temperamental aspects of personality and emotions. Specifically, lower PD_{pulse} was positively associated with positive personality measures of agreeableness, conscientiousness, and extroversion and negatively associated with negative personality measure of neuroticism ($p < 0.02$; 2-tailed; Supplementary Tables S2). In the same way, PD_{pulse} was associated with emotion test scores in negative affect, psychological well-being, social relationships, and stress instruments (e.g., PD_{pulse} correlated positively with perceived stress test and negatively with self-efficacy test of the stress instrument; Supplementary Table S3).

PD_{pulse} was also significantly reproducible within subjects (ICC(3, 1) = 0.23, $F(202, 606) = 2.18$, $p < 0.00001$). Controlling for age did not affect the associations between PD_{pulse} and personality PC ($r(201) = 0.31$, $p < 0.00001$) and emotion PC ($r(201) = 0.23$, $p = 0.0011$). Gender was not associated with PD_{pulse} nor with personality and emotion PCs ($p > 0.2$). Similar analyses on the respiratory amplitude fluctuations showed that the correlations between PD_{resp} and personality and emotion PCs were not significant ($p > 0.2$). We also did not find significant correlations between PD of respiratory rate or PD of pulse-rate (Supplementary Fig. S3*b*) and personality or emotion PCs ($p > 0.12$). In addition, average amplitude of LFR coherence between pulse and RSNs signals was not significantly correlated with personality and emotion PCs ($p > 0.3$). However,

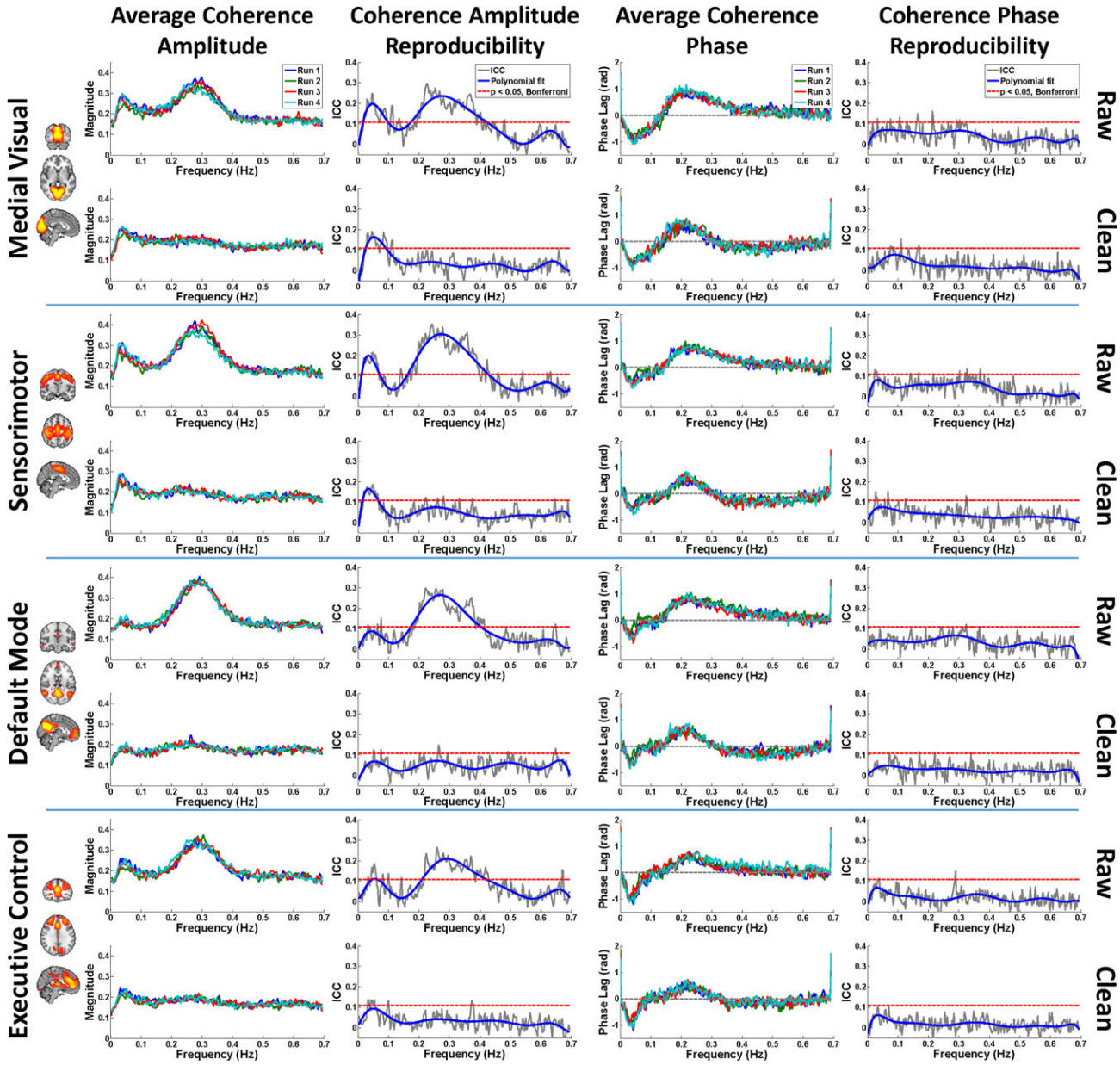

Figure 3. Amplitude and phase associations between RSNs and respiratory amplitude fluctuations. First column shows the amplitude of coherence between RSNs and respiratory signals for different frequency bins (n = 256), averaged across subjects for each fMRI run for raw (top row) and clean (bottom row) datasets. The within-subject reproducibility of these amplitude associations for each frequency bin was characterized using ICC(3, 1). The third column shows the coherence phase for each frequency bin averaged across subjects for each run, followed by the fourth column showing within-subject reproducibility of these phase measures for raw and clean datasets.

average phase of LFR coherence between pulse and RSN was significantly associated with personality ($r(201) = -0.193$, $p = 0.0057$) and emotion ($r(201) = -0.1465$, $p = 0.0370$) PCs. Since head motion is increasingly recognized as an important contributor to patterns of brain activity and has been linked to behavioral phenotypes (Kong et al. 2014; Zeng et al. 2014; Hodgson et al. 2016), we assessed the extent to which head motion contributes to our results. Average framewise displacement (FD) (Power et al. 2012) across the 4 runs (M = 0.17 mm, SD = 0.05 mm) was not associated with personality and emotion PCs ($p > 0.5$), but FD was associated with the motor PC ($r(201) = -0.28$; $p < 0.0001$), particularly, higher FD predicted lower endurance and dexterity instrument scores.

Finally, we mapped the distribution of PD_{pulse} at the voxel level (Fig. 6*a*) to highlight regions showing greater interactions with pulse amplitude fluctuations (indexing sympathetic tone). This "autonomic network" included sensorimotor, visual, and auditory cortices (but not the language network), along with parts of posterior cingulate, precuneus, parahippocampal gyrus, hippocampus, and thalamus, that showed relatively higher PD_{pulse} than the rest of the brain ($p_{FWE} < 0.05$; Supplementary Table S16). Average PD_{pulse} within this autonomic network was associated with personality PC ($r(201) = 0.29$, $p = 0.00002$) and emotion PC ($r(201) = 0.19$, $p = 0.006$). We also performed a voxelwise correlation analysis to determine regions with the greatest association between PD_{pulse} and

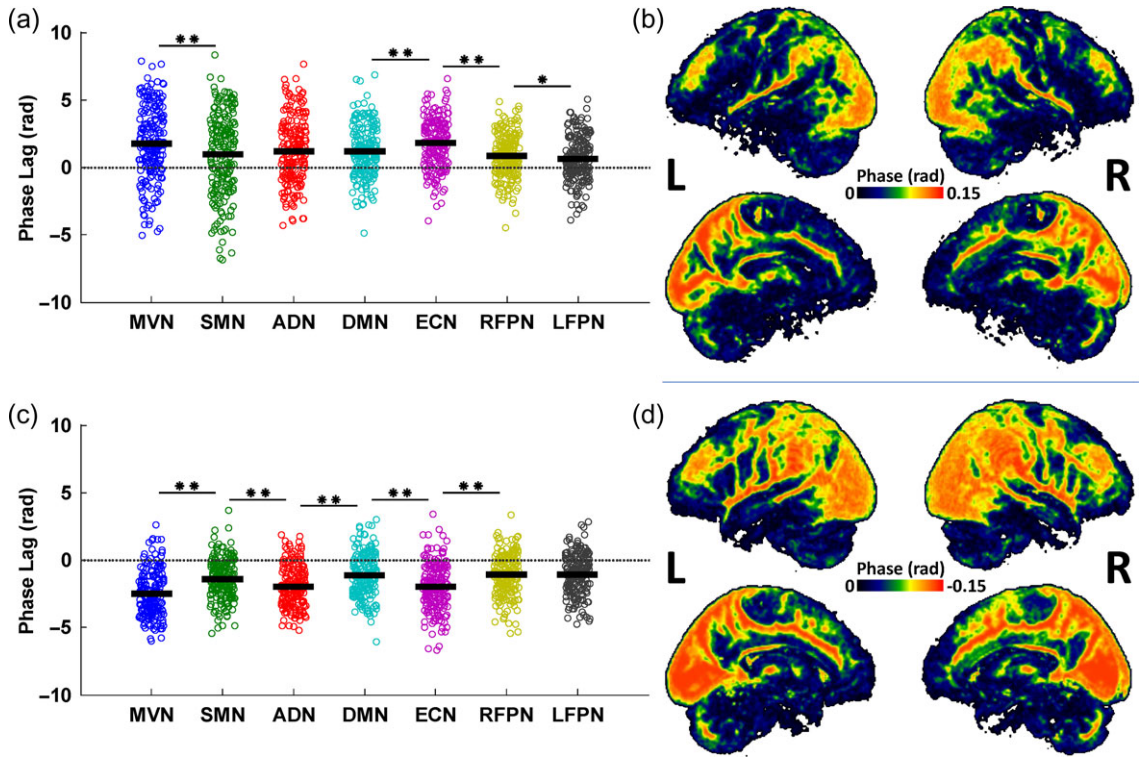

Figure 4. Average phase lag across 4 fMRI runs for pulse and respiratory amplitude fluctuations relative to RSNs at LFs (0.01–0.09 Hz). (*a*) Distribution of subjects' average phase (across 4 runs) relative to pulse signal shown for MVN, SMN, ADN, DMN, ECN, RFPN, and LFPN. The dark thick lines show the group average of phase estimates and the thin lines show significant pairwise differences between RSN phase estimates. The positive phase for all networks indicated that the pulse amplitude fluctuations preceded those in the brain. The networks varied in their phase lag relative to pulse amplitude fluctuations ($F(4.04, 816.47) = 16.79$, $p < 0.0001$; $^{*}p = 0.056$, $^{**}p < 0.0001$, 2-tailed). (*b*) Lateral (top) and medial (bottom) views of phase lag of pulse amplitude fluctuations relative to resting brain fluctuations calculated for each voxel individually and averaged over 4 runs. (*c*) Phase lag of respiratory amplitude fluctuations relative to RSNs. The negative lag indicates that the respiratory amplitude fluctuations follow those in the brain. The networks varied in their phase lag relative to respiratory amplitude fluctuations ($F(5.19, 1049.11) = 42.46$, $p < 0.0001$; $^{**}p < 0.0001$, 2-tailed). (*d*) Lateral (top) and medial (bottom) views of phase lag of respiratory amplitude fluctuations relative to resting brain fluctuations calculated for each voxel individually and averaged over 4 runs.

personality and emotion PCs (Fig. 6*b*, *c*). Areas showing PD_{pulse} associations with both personality and emotion PCs included medial and superior frontal gyrus as well as cuneus and lingual gyrus. Personality PC was also significantly correlated with bilateral inferior frontal gyrus and precuneus ($p_{FWE} < 0.05$, Supplementary Tables S17 and S18).

Discussion

Here we show that the consistency in the temporal associations between brain RSNs and pulse amplitude fluctuations in LFR was associated with a main positivity/negativity dimension of human personality and emotions. Lack of an association between PD_{resp} and the same personality and emotion PCs supported the specificity of this phenomenon for PD_{pulse}. We also did not find significant associations between PD of respiratory-rate variability or pulse-rate variability and personality or emotions indicating that the identified brain-pulse interactions are directly related to pulse amplitude fluctuations in the LFR (presumed to be an indirect index of sympathetic activity) (Nitzan et al. 1996; Mizeva et al. 2015) rather than fluctuations in the pulse rate (associated with both sympathetic and parasympathetic activity) (Houle and Billman 1999; Stauss 2003). We also found associations between the average of pulse-RSNs phase lag (in LFR) and emotions and personality. These effects were not as strong as those for PD_{pulse}, but it is worth noting that the pulse-RSNs phase lag (delay) could be affected by additional factors such as body size or blood pressure (He and Goubran 2013).

Personality–Emotion "*g*" factor (G_{PE})

From a behavioral perspective, we found that a large amount of variance in personality (first PC: $R^2 = 0.42$) and emotion (first PC: $R^2 = 0.33$) measures (Supplementary Fig. S1) fall along a main dimension of positivity and negativity (Supplementary Tables S2 and S3). Interestingly, these PCs were highly correlated ($r(201) = 0.69$) but were unrelated to PCs of other behavioral categories (see Section Behavioral Assessments). As expected, many personality factors and measures of emotion (e.g., both positive and negative affects) were correlated with these PCs (Supplementary Tables S2 and S3). Despite clear indications that there are distinct personality factors (e.g., the 5-factor model) (Goldberg 1993) and emotional depositions (e.g., positive versus negative affects) (Diener and Emmons 1984), our behavioral analysis suggested that these measures still share common variance (G_{PE}) (Schmukle et al. 2002; Revelle and Wilt 2013). The personality PC and PD_{pulse} were similarly related to all personality factors (except "Openness to experience") (Supplementary Table S2). The emotion PC was not related to

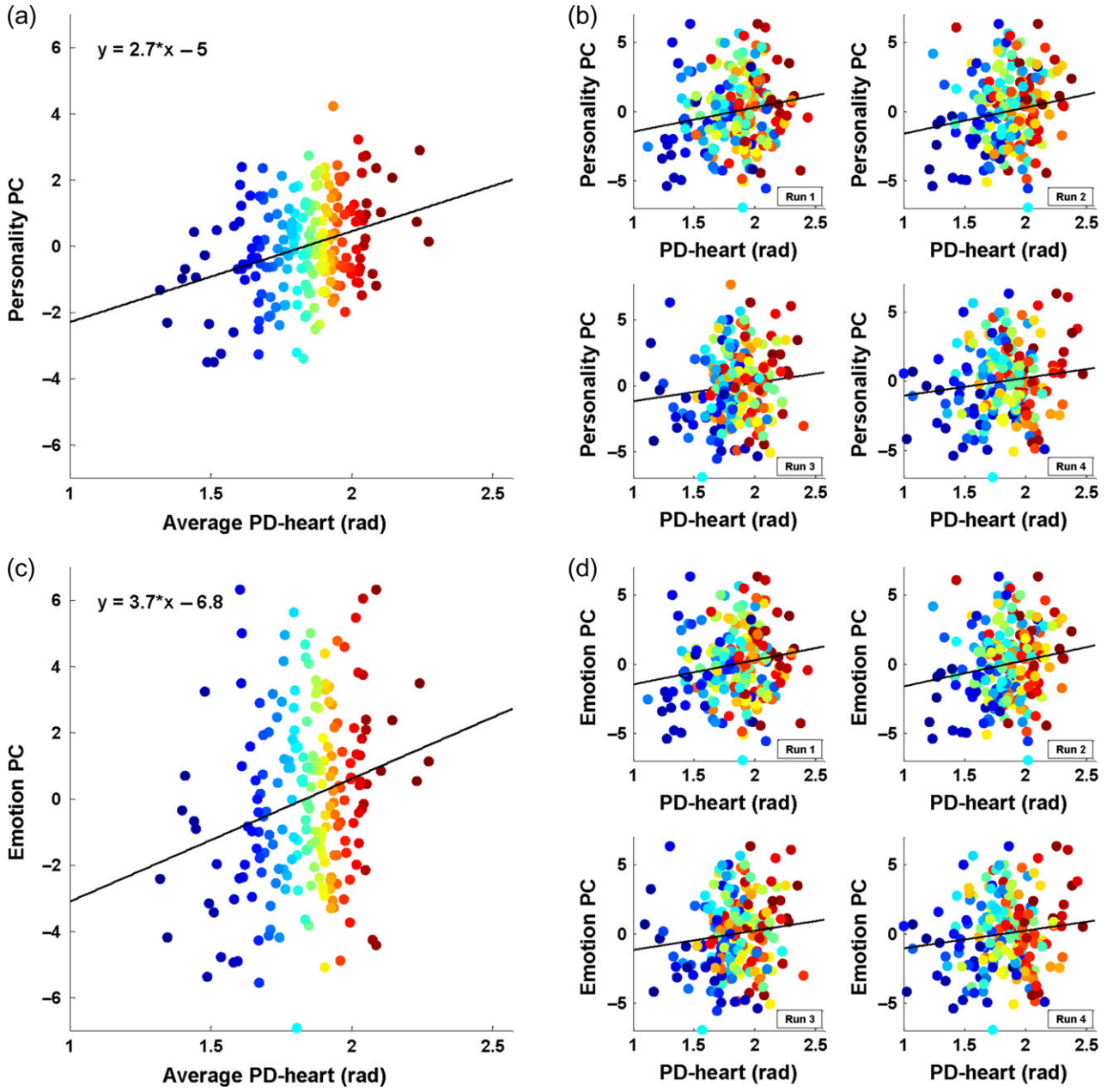

Figure 5. Association between the PD relative to pulse amplitude fluctuations (PD_{pulse}; 0.01–0.09 Hz) and personality and emotion PCs. (*a*) The scatter plot of average PD_{pulse} across 4 runs across 7 RSNs for each subject and the corresponding personality PC score. Subjects are color coded from blue to red for low to high PD_{pulse}. (*b*) Subjects' PD_{pulse} for each run plotted against personality PC score. Subjects are color coded based on their relative PD_{pulse} rank in part (*a*). (*c*) Average PD_{pulse} across 4 runs for subjects and their corresponding emotion PC score. (*d*) Subjects' PD_{pulse} for each run plotted against emotion PC score.

the emotion identification tasks but was related to measures of one's own emotional experience. In the same way, PD_{pulse} was associated with measures of self-relevant emotional experience, including the experience of primary emotions (sadness, anger-hostility) as well as self-reflection on more complex constructs of self-identity (e.g., life satisfaction, meaning and purpose, and self-efficacy) (Supplementary Table S3). The association between PD_{pulse} and personality and emotion PCs suggests that PD_{pulse} may inform biological determinants of G_{PE}, which are likely related to autonomic signaling of the cortex (Fig. 6).

RSN Spatiotemporal Characteristics

We characterized spatiotemporal characteristics of RSNs as well as the amplitude and phase of their coherence with pulse and respiratory amplitude fluctuations. We showed that despite significant within-subject spatial reproducibility in the anatomical location of RSNs, the LFR which accounted for most of the RSN spectral power, was not reproducible within subjects (Supplementary Table S12). While the nature of the slow-rate RSN fluctuations is still unclear, it has been postulated that they reflect inter and intraregional oscillatory processes (Li

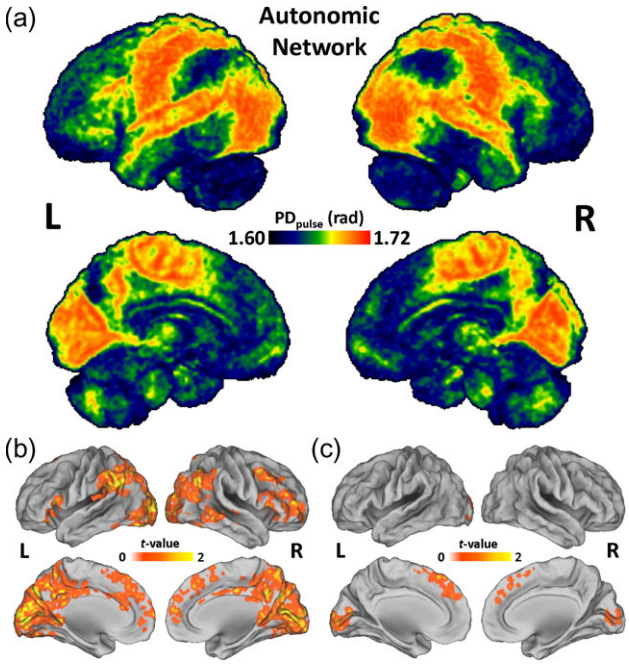

Figure 6. Autonomic network: phase dispersion (PD_{pulse}) map for pulse signal and associations with personality and emotions. (*a*) Lateral (top) and medial (bottom) views of voxel-level average of PD_{pulse} (0.01–0.09 Hz) across the 4 fMRI runs and the 203 participants in each voxel (no underlay image used). PD_{pulse} was calculated for each brain voxel, independently, highlighting the brain regions within the autonomic network with higher interactions peripheral signals. See Supplementary Table S16 for the list of regions with significantly higher PD_{pulse} than the rest of the brain. (*b*) Lateral (top) and medial (bottom) views of regions showing significant correlation ($p_{FWE} < 0.05$) between PD_{pulse} and first PC of personality category (see Supplementary Tables S2 and S17). (*c*) Lateral (top) and medial (bottom) views of regions showing significant correlation ($p_{FWE} < 0.05$) between PD_{pulse} and first PC of emotion category (see Supplementary Tables S3 and S18).

et al. 2015) or emergent fluctuations reflecting complex dynamic interactions between brain networks (Honey et al. 2007; Deco et al. 2013) and body physiology (Nikolaou et al. 2016). Notwithstanding the fact that most of the RSN's spectral power is concentrated in LFR (Supplementary Table S11), the lack of significant reproducibility in the spectral content of LFR (relative to MFR) (Fig. 1 and Supplementary Fig. S2) does not support that RSN's activity is driven by fixed (or reproducible) slow-rate temporal rhythms (Li et al. 2015; Wang et al. 2016). Instead, significant associations between physiological signals and the sensory RSNs suggest a modulatory effect of body physiology, particularly slow pulse amplitude fluctuations, on RSNs. Specifically, we found that respiratory and pulse fluctuations interact differently with the RSN fluctuations in different frequency bands (Figs 2 and 3, Supplementary Figs S4 and S5), an effect that was more pronounced in sensory-related RSNs. For LFR, there were reproducible amplitudes of coherence between these slow fluctuations in sensory RSNs and those in pulse and respiratory amplitude fluctuations (Figs 2 and 3, Supplementary Figs S3 and S4). The analysis of spectral content of pulse amplitude fluctuations identified a distinct peak at 0.07 Hz (Supplementary Fig. S3), suggesting that a separate source (e.g., slow components of vasomotion) (Turalska et al. 2008) may contribute to pulse amplitude fluctuations in LFR.

Nature of LFR Pulse Amplitude Fluctuations

Our analysis on the associations between ECG and left- and right-hand pulse signals (Supplementary Fig. S6) indicated a significant correspondence between LFR amplitude fluctuations of the left- and right-hand pulse recordings, but not between the LFR amplitude fluctuations of the ECG and pulse recordings. This observation is consistent with the notion that LFR pulse amplitude fluctuations reflect a vascular phenomenon that is likely not related to electrical cardiac activity. In contrast to the parasympathetic system, the sympathetic system mediates vasoconstriction in arteries and veins (Klabunde 2011). Accordingly, LF amplitude fluctuations in the pulse signal (reflecting vessel elasticity) have been suggested as an indirect index of sympathetic activity (Nitzan et al. 1996; Murphy et al. 2013; Mizeva et al. 2015). Considering that sympathetic tone does not uniformly affect body vasculature, our data uncover that low-frequency synchrony between brain RSNs and pulse (PD_{pulse}) is variable between participants (Fig. 5), which might reflect individual differences in (simultaneous) modulation of cerebral and peripheral vessels by the sympathetic activity. While we primarily attributed the LFR amplitude fluctuations of the pulse to sympathetic activity, it will be important in the future to differentiate the contributions of sympathetic and parasympathetic activity to physiological signals (Galante 2009; Macey, Rieken, et al. 2016) and to characterize their common and unique influence on regional brain activity. In addition, mechanisms mediating LFR amplitude fluctuations remain to be explored. For example, the locus coeruleus (LC) of the brainstem, as a part of ascending reticular activating system, plays a central role in the homeostatic control of the body, particularly mediating sympathetic tone in a range of conditions such as stress (Samuels and Szabadi 2008). LC has wide projections to central and peripheral nervous system but receives inputs from a limited set of brain regions including the medial frontal regions where we also found low PD_{pulse} and significant associations between PD_{pulse} and personality PC and emotion PC (Fig. 6, Supplementary Tables S16–S18). Yet, the relevance of LC to our findings demands further research.

Biological Determinants of PD_{pulse}

The physiological nature of our observations (PD_{pulse}) and recent genetic findings (Smith et al. 2016) suggest that an aspect of personality and emotions (the positivity/negativity dimension) may be biologically predetermined (or hardwired). It is also possible that environmental variables such as exposure to stressors (particularly during brain development) would be associated with changes in the sympathetic tone (and its potential interaction with personality and emotions) (Quas et al. 2014). Future work should investigate the contribution of common genetic factors involved in sympathetic activity, vascular signaling, reactivity to stressors, and personality and emotions (Smith et al. 2016). Demographic factors such as gender and age are also related to sympathetic function (Hinojosa-Laborde et al. 1999; Hart et al. 2009). Despite the evidence suggesting significant gender differences in measures of sympathetic activity and its fMRI correlates (Macey, Rieken, et al. 2016), we did not find a significant association between PD_{pulse} and gender. Noting the limited age range in our data (22–35 years), age was not associated with PD_{pulse}, but future work will be needed to assess age effects in a wider age range.

An Autonomic Network

The phase analyses between RSNs and physiology revealed that there is consistency in the temporal order of RSN–physiology interactions, with LFR fluctuations in pulse recordings preceding those in RSNs (Fig. 4*a*), and LFR respiratory amplitude fluctuations following those in RSNs (Fig. 4*c*). Though recent evidence suggests that RSNs emerge from a composite of lag threads (Mitra et al. 2015), our data revealed that many RSNs have different phase lags relative to body physiology (Fig. 4). Future work could investigate the extent to which different interactions with physiological fluctuations might contribute to emergence of distinct RSNs. The phase maps for brain fluctuations relative to pulse and respiration highlight major arterial and venous pathways (e.g., divisions of the middle and anterior cerebral artery are clearly distinguished in Fig. 4*b* and 4*d*), suggesting that vascular pathways mediate the physiological associations with brain resting activity. The voxel-level PD_{pulse} map (Fig. 6*a*, Supplementary Table S16) primarily highlighted the posterior regions including sensory (and motor) cortices and the dorsal attention stream, suggesting that these regions may be considered as the basis of an "autonomic brain network" within which there are stronger interactions with the pulse amplitude fluctuations (indexing sympathetic activity) than the rest of the brain. Interestingly, PD_{pulse} within this autonomic network was also associated with personality and emotion PCs. Voxel-level mapping of the associations between PD_{pulse} and PCs of personality and emotion consistently revealed areas within the visual and medial prefrontal cortices. While visual and medial frontal cortices have been associated with emotions (Lang et al. 1998; Etkin et al. 2011), our results highlight that autonomic control of vasculature in these regions should be considered when characterizing their contribution to emotions and personality. Our findings could be interpreted so that vascular signaling might influence brain activity, particularly in this autonomic network which may be related to aspects of interoceptive processing. Possible mechanisms are unclear but could involve vascular-induced stimulation of neuronal or glial transient receptor potential channels (Moore and Cao 2008; Zhang and Liao 2015) as well as other mechanosensitive ion channels (e.g., potassium channels TREK-1 and TRAAK) in neuronal membranes (Kubanek et al. 2016).

MFR and HFR of fMRI

In the MFR (0.1–0.2 Hz), sensory RSNs exhibited significant reproducibility, with rhythms in this frequency range being consistently present within individuals (Fig. 1, Supplementary Fig. S2, Supplementary Table S12). This frequency range overlaps with the range of frequencies implicated in the coherence of resting pulsation of arterioles (0.1–1.0 Hz) (Drew et al. 2011; Du et al. 2014) and cerebral vasomotion (0.1 Hz) (Mayhew et al. 1996; Nikulin et al. 2014). However, this phenomenon does not explain why the effects were more pronounced in sensory RSNs. It may be that sensory RSNs, relative to higher order RSNs, more consistently follow the distribution of main arterial pathways and therefore are more sensitive to reflecting these vascular pulsatory phenomena (Başar and Weiss 1981). In the HFR (0.2–0.7 Hz), we observed significant reproducibility for the frequency amplitudes across all RSNs in the raw data (Supplementary Table S13). In addition, the magnitude of coherence between physiological and RSN fluctuations was also reproducible. However, these effects were no longer detected after removing the physiologically driven components from RSN time courses (see Section Methods). When considering the phase information, we inferred that respiratory amplitude fluctuations in this band precede the fluctuation in RSNs (Fig. 3, Supplementary Fig. S5), indicating that these effects are primarily driven by respiration. This finding suggests that spontaneous fluctuations in the BOLD signal (particularly within 0.2–0.5 Hz) may reflect changes in the blood oxygenation due to respiration and expands on similar findings in the lower frequency ranges (Chang and Glover 2009; Yuan et al. 2013). There is evidence that respiration modulates oscillatory activity of neurons in the olfactory cortex both through airflow-dependent and -independent mechanisms (Phillips et al. 2012). However, the modulation of RSN activity by respiration might be independent of the effect of breathing on the olfactory system. For example, activation of the sensorimotor cortex is part of the respiratory-related evoked potential detected by EEG (von Leupoldt et al. 2010) and oscillatory activity (0.5–4 Hz) in the whisker barrel cortical field in the mouse brain is also modulated by respiration (Ito et al. 2014). Similarly, pain perception is influenced by respiration (Iwabe et al. 2014; Reyes del Paso et al. 2015). Since context influences sensory processing, it is likely that physiological information relevant to the state of the body is an important modulator of cortical activity (Juravle et al. 2014).

Methodological Considerations and Limitations

Although the temporal lag between pulse and RSN fluctuations suggests pulse amplitude fluctuations may drive LFR RSNs' activity, at this stage, we are not able to demonstrate causality (Moore and Cao 2008). Experimental manipulations of PD_{pulse} and their effect on personality and emotions are needed to establish causality (Feldman et al. 2010; Kim et al. 2013; Holper et al. 2015; Steinhubl et al. 2015). Our study was limited to monitoring the peripheral signals only through the PPG and respiratory recordings. Although, high-quality ECG recordings of cardiac electrical activity in MRI are not reliable due to significant MR-related artifacts (Wong et al. 2011) and are potentially hazardous (Kugel et al. 2003), alternative means for monitoring cardiovascular function such as blood pressure measures (e.g., with indwelling catheters) and measures of sympathetic activity (e.g., sympathetic skin response) and parasympathetic activity (e.g., heart-rate variability) should be considered for future studies (Macey, Ogren, et al. 2016). Physiological data recording is highly prone to noise (e.g., because of subject motion or improper device attachments), which may severely affect the signals. Detrending or despiking technique could be applied to mitigate these problems. In addition, it is critical to maintain the physiological signal recording in exact synchrony with fMRI data acquisition, especially when phase information is being studied. Finally, higher fMRI sampling rates (>3 Hz) will be needed to alleviate aliasing of heart-related frequency content into lower frequency bands.

Conclusions

The relevance of physiological signals in emotions is well recognized. As described by Damasio and Carvalho (2013), "Survival depends on the maintenance of the body's physiology within an optimal homeostatic range. This process relies on fast detection of potentially deleterious changes in body state and on appropriate corrective responses." Our results highlight that an important aspect of personality and emotions could be related to interactions within a network of peripheral signals and brain regions (autonomic network) and point at the

importance of studying the interactions between the central and autonomic nervous systems for characterizing personality and emotions. Presumably, synchronous effect of sympathetic tone (regulating homeostasis) on cerebral and peripheral vasculature, combined with the quality of neurovascular coupling (the brain's sensitivity to vascular signaling), may shape a main dimension of personality and emotions. Finally, understanding how brain–body interactions affect human personality and emotions is of relevance to guide therapeutic interventions in related psychiatric disorders and to inspire behavioral interventions for improving well-being.

Supplementary Material

Supplementary material is available at *Cerebral Cortex* online.

Authors' Contributions

E.S.-K. initiated the study, developed the techniques, performed the analyses, and wrote most of the paper. N.D.V. reviewed the analyses and wrote the paper. D.T. reviewed the analyses and edited the paper. All authors discussed the results.

Funding

HCP data were provided by WU-Minn Consortium (PIs: David Van Essen and Kamil Ugurbil; 1U54MH091657-01) funded by 16 NIH institutes and centers that support the NIH Blueprint for Neuroscience Research and by the McDonnell Center for Systems Neuroscience at Washington University. This work was supported by the intramural research program of the National Institute on Alcohol Abuse and Alcoholism (Grant Y1AA-3009).

Notes

We thank Catie Chang, Sukru Baris Demiral, and Carrie McAdams for helpful comments, Gene-Jack Wang, Corinde Wiers, and Peter Manza for their support and Elizabeth Cabrera for assistance with manuscript preparation. We thank Veronica Ramirez, Gregg Miller, Minoo McFarland, and Lori Talagala for assistance with subject recruitment and/or data collection at the NIH. We thank Karen Torres and Christopher Wong for administrative support. This study utilized the high-performance computational capabilities of the Biowulf Linux cluster at NIH (http://biowulf.nih.gov). For further data and analysis details please see: https://github.com/eshoko/BBI. *Conflict of Interest*: None declared.

References

Allen J. 2007. Photoplethysmography and its application in clinical physiological measurement. Physiol Meas. 28:R1.

Awad AA, Ghobashy MAM, Ouda W, Stout RG, Silverman DG, Shelley KH. 2001. Different responses of ear and finger pulse oximeter wave form to cold pressor test. Anesth Analg. 92: 1483–1486.

Başar E, Weiss C. 1981. Vasculature and circulation: the role of myogenic reactivity in the regulation of blood flow. Great Britain: Elsevier Science Ltd.

Beckmann CF, DeLuca M, Devlin JT, Smith SM. 2005. Investigations into resting-state connectivity using independent component analysis. Philos Trans R Soc Lond B Biol Sci. 360:1001–1013.

Beckmann CF, Smith SM. 2004. Probabilistic independent component analysis for functional magnetic resonance imaging. IEEE Trans Med Imaging. 23:137–152.

Bolanos M, Nazeran H, Hltiwanger E. 2016. Comparison of heart rate variability signal features derived from electrocardiography and photoplethysmography in healthy individuals. Eng Med Biol Soc. 4289–4294.

Brener J, Ring C. 2016. Towards a psychophysics of interoceptive processes: the measurement of heartbeat detection. Phil Trans R Soc B. 371:20160015.

Brodal P. 2004. The central nervous system: structure and function. USA: Oxford University Press.

Calhoun V, Adali T, Pearlson G, Pekar J. 2001. Spatial and temporal independent component analysis of functional MRI data containing a pair of task-related waveforms. Hum Brain Mapp. 13:43–53.

Chan GS, Tang CH, Middleton PM, Cave G, Harvey M, Savkin AV, Lovell NH. 2010. Augmented photoplethysmographic low frequency waves at the onset of endotoxic shock in rabbits. Physiol Meas. 31:1605.

Chang C, Glover GH. 2009. Relationship between respiration, end-tidal CO 2, and BOLD signals in resting-state fMRI. Neuroimage. 47:1381–1393.

Costa PT, McCrae RR, Psychological Assessment Resources I. 1992. Revised NEO Personality Inventory (NEO PI-R) and NEO Five-Factor Inventory (NEO-FFI): Psychological Assessment Resources.

Craig AD. 2009. How do you feel—now? the anterior insula and human awareness. Nat Rev Neurosci. 10:59–70.

Critchley HD, Wiens S, Rotshtein P, Öhman A, Dolan RJ. 2004. Neural systems supporting interoceptive awareness. Nat Neurosci. 7:189–195.

Damasio A, Carvalho GB. 2013. The nature of feelings: evolutionary and neurobiological origins. Nat Rev Neurosci. 14: 143–152.

De Pascalis V, Cozzuto G, Caprara GV, Alessandri G. 2013. Relations among EEG-alpha asymmetry, BIS/BAS, and dispositional optimism. Biol Psychol. 94:198–209.

Deco G, Ponce-Alvarez A, Mantini D, Romani GL, Hagmann P, Corbetta M. 2013. Resting-state functional connectivity emerges from structurally and dynamically shaped slow linear fluctuations. J Neurosci. 33:11239–11252.

Denollet J, Pedersen SS, Vrints CJ, Conraads VM. 2006. Usefulness of type D personality in predicting five-year cardiac events above and beyond concurrent symptoms of stress in patients with coronary heart disease. Am J Cardiol. 97:970–973.

Depue RA, Luciana M, Arbisi P, Collins P, Leon A. 1994. Dopamine and the structure of personality: relation of agonist-induced dopamine activity to positive emotionality. J Pers Soc Psychol. 67:485.

Diener E, Emmons RA. 1984. The independence of positive and negative affect. J Pers Soc Psychol. 47:1105.

Drew PJ, Shih AY, Kleinfeld D. 2011. Fluctuating and sensory-induced vasodynamics in rodent cortex extend arteriole capacity. Proc Natl Acad Sci U S A. 108:8473–8478.

Du C, Volkow ND, Koretsky AP, Pan Y. 2014. Low-frequency calcium oscillations accompany deoxyhemoglobin oscillations in rat somatosensory cortex. Proc Natl Acad Sci USA. 111: E4677–E4686.

Duschek S, Wörsching J, Reyes del Paso GA. 2015. Autonomic cardiovascular regulation and cortical tone. Clin Physiol Funct Imaging. 35:383–392.

Etkin A, Egner T, Kalisch R. 2011. Emotional processing in anterior cingulate and medial prefrontal cortex. Trends Cogn Sci. 15:85–93.

Feldman G, Greeson J, Senville J. 2010. Differential effects of mindful breathing, progressive muscle relaxation, and loving-kindness meditation on decentering and negative reactions to repetitive thoughts. Behav Res Ther. 48: 1002–1011.

Fredrickson BL, Levenson RW. 1998. Positive emotions speed recovery from the cardiovascular sequelae of negative emotions. Cogn Emot. 12:191.

Gabard-Durnam LJ, Flannery J, Goff B, Gee DG, Humphreys KL, Telzer E, Hare T, Tottenham N. 2014. The development of human amygdala functional connectivity at rest from 4 to 23 years: a cross-sectional study. Neuroimage. 95:193–207.

Galante NJ. 2009. Photoplethysmographic waveform analysis during lower body negative pressure simulated hypovolemia as a tool to distinguish regional differences in microvascular blood flow regulation.

Gershon RC, Cella D, Fox NA, Havlik RJ, Hendrie HC, Wagster MV. 2010. Assessment of neurological and behavioural function: the NIH Toolbox. Lancet Neurol. 9:138–139.

Gil E, Vergara JM, Laguna P. 2008. Detection of decreases in the amplitude fluctuation of pulse photoplethysmography signal as indication of obstructive sleep apnea syndrome in children. Biomed Signal Process Control. 3:267–277.

Glasser MF, Sotiropoulos SN, Wilson JA, Coalson TS, Fischl B, Andersson JL, Xu J, Jbabdi S, Webster M, Polimeni JR. 2013. The minimal preprocessing pipelines for the Human Connectome Project. Neuroimage. 80:105–124.

Goldberg LR. 1993. The structure of phenotypic personality traits. Am Psychol. 48:26.

Gray MA, Beacher FD, Minati L, Nagai Y, Kemp AH, Harrison NA, Critchley HD. 2012. Emotional appraisal is influenced by cardiac afferent information. Emotion. 12:180.

Hamel E. 2006. Perivascular nerves and the regulation of cerebrovascular tone. J Appl Physiol. 100:1059–1064.

Harper AM, Deshmukh VD, Rowan JO, Jennett WB. 1972. The influence of sympathetic nervous activity on cerebral blood flow. Arch Neurol. 27:1–6.

Hart EC, Joyner MJ, Wallin BG, Johnson CP, Curry TB, Eisenach JH, Charkoudian N. 2009. Age-related differences in the sympathetic-hemodynamic balance in men. Hypertension. 54:127–133.

He X, Goubran RA, Liu XP, editors. 2013. Year Published|. Title|, Conference Name|; Year of Conference Date|; Conference Location| Place Published|:Publisher|. Pages p|.

Hinojosa-Laborde C, Chapa I, Lange D, Haywood JR. 1999. Gender differences in sympathetic nervous system regulation. Clin Exp Pharmacol Physiol. 26:122–126.

Hodgson K, Poldrack RA, Curran JE, Knowles EE, Mathias S, Göring HH, Yao N, Olvera RL, Fox PT, Almasy L. 2016. Shared genetic factors influence head motion during MRI and body mass index. Cereb Cortex. 27(12):5539–5546.

Holper L, Scholkmann F, Seifritz E. 2015. Time–frequency dynamics of the sum of intra-and extracerebral hemodynamic functional connectivity during resting-state and respiratory challenges assessed by multimodal functional near-infrared spectroscopy. Neuroimage. 120:481–492.

Homma I, Masaoka Y. 2008. Breathing rhythms and emotions. Exp Physiol. 93:1011–1021.

Honey CJ, Kötter R, Breakspear M, Sporns O. 2007. Network structure of cerebral cortex shapes functional connectivity on multiple time scales. Proc Natl Acad Sci USA. 104: 10240–10245.

Hopkins WG. 2000. Measures of reliability in sports medicine and science. Sports Med. 30:1–15.

Houle MS, Billman GE. 1999. Low-frequency component of the heart rate variability spectrum: a poor marker of sympathetic activity. Am J Physiol-Heart Circ Physiol. 276:H215–H223.

Ito J, Roy S, Liu Y, Cao Y, Fletcher M, Lu L, Boughter J, Grün S, Heck D. 2014. Whisker barrel cortex delta oscillations and gamma power in the awake mouse are linked to respiration. Nat Commun. 5:3572.

Iwabe T, Ozaki I, Hashizume A. 2014. The respiratory cycle modulates brain potentials, sympathetic activity, and subjective pain sensation induced by noxious stimulation. Neurosci Res. 84:47–59.

Jenkins CD, Rosenman RH, Zyzanski SJ. 1974. Prediction of clinical coronary heart disease by a test for the coronary-prone behavior pattern. N Engl J Med. 290:1271–1275.

Jennings JR, Sheu LK, Kuan DCH, Manuck SB, Gianaros PJ. 2015. Resting state connectivity of the medial prefrontal cortex covaries with individual differences in high-frequency heart rate variability. Psychophysiology. 53(4):444–54.

Juravle G, Stoeckel MC, Rose M, Gamer M, Büchel C, Wieser MJ, von Leupoldt A. 2014. Investigating the effect of respiratory bodily threat on the processing of emotional pictures. Respir Physiol Neurobiol. 204:41–49.

Katkin ES, Blascovich J, Goldband S. 1981. Empirical assessment of visceral self-perception: individual and sex differences in the acquisition of heartbeat discrimination. J Pers Soc Psychol. 40:1095.

Kay SM 1988. Modern Spectral Estimation: Theory and Application/Book and Disk: PTR Prentice Hall.

Kim D, Kang SW, Lee K-M, Kim J, Whang M-C. 2013. Dynamic correlations between heart and brain rhythm during autogenic meditation. Front Hum Neurosci. 7:414.

Kim C-J, Whang M-C, Kim J-H, Woo J-C, Kim Y-W, Kim J-H. 2010. A study on evaluation of human arousal level using PPG analysis. J Ergon Soc Korea. 29:113–120.

Klabunde R. 2011. Cardiovascular physiology concepts. USA: Lippincott Williams & Wilkins.

Kong X-z, Zhen Z, Li X, Lu H-h, Wang R, Liu L, He Y, Zang Y, Liu J. 2014. Individual differences in impulsivity predict head motion during magnetic resonance imaging. PLoS One. 9: e104989.

Kop WJ, Synowski SJ, Newell ME, Schmidt LA, Waldstein SR, Fox NA. 2011. Autonomic nervous system reactivity to positive and negative mood induction: the role of acute psychological responses and frontal electrocortical activity. Biol Psychol. 86:230–238.

Kreibig SD. 2010. Autonomic nervous system activity in emotion: a review. Biol Psychol. 84:394–421.

Kubanek J, Shi J, Marsh J, Chen D, Deng C, Cui J. 2016. Ultrasound modulates ion channel currents. Sci Rep. 6:24170.

Kugel H, Bremer C, Püschel M, Fischbach R, Lenzen H, Tombach B, Van Aken H, Heindel W. 2003. Hazardous situation in the MR bore: induction in ECG leads causes fire. Eur Radiol. 13: 690–694.

Landsverk SA, Kvandal P, Bernjak A, Stefanovska A, Kirkeboen KA. 2007. The effects of general anesthesia on human skin microcirculation evaluated by wavelet transform. Anesth Analg. 105:1012–1019.

Lang PJ, Bradley MM, Fitzsimmons JR, Cuthbert BN, Scott JD, Moulder B, Nangia V. 1998. Emotional arousal and activation

of the visual cortex: an fMRI analysis. Psychophysiology. 35: 199–210.

LeBlanc J, Ducharme M, Thompson M. 2004. Study on the correlation of the autonomic nervous system responses to a stressor of high discomfort with personality traits. Physiol Behav. 82:647–652.

Lesch K-P, Araragi N, Waider J, van den Hove D, Gutknecht L. 2012. Targeting brain serotonin synthesis: insights into neurodevelopmental disorders with long-term outcomes related to negative emotionality, aggression and antisocial behaviour. Phil Trans R Soc B. 367:2426–2443.

Lester D. 2012. The autonomic nervous system and personality. Psychol Rep. 111:44–46.

Li JM, Bentley WJ, Snyder AZ, Raichle ME, Snyder LH. 2015. Functional connectivity arises from a slow rhythmic mechanism. Proc Natl Acad Sci USA. 112:E2527–E2535.

Macey PM, Ogren JA, Kumar R, Harper RM. 2016a. Functional imaging of autonomic regulation: methods and key findings. Front Neurosci. 9:513.

Macey PM, Rieken NS, Kumar R, Ogren JA, Middlekauff HR, Wu P, Woo MA, Harper RM. 2016b. Sex differences in insular cortex gyri responses to the Valsalva maneuver. Front Neurol. 7:87.

Marins FR, Limborco-Filho M, Xavier CH, Biancardi VC, Vaz GC, Stern JE, Oppenheimer SM, Fontes MA. 2016. Functional topography of cardiovascular regulation along the rostrocaudal axis of the rat posterior insular cortex. Clin Exp Pharmacol Physiol. 43:484–493.

Mayhew JE, Askew S, Zheng Y, Porrill J, Westby GM, Redgrave P, Rector DM, Harper RM. 1996. Cerebral vasomotion: a 0.1-Hz oscillation in reflected light imaging of neural activity. Neuroimage. 4:183–193.

McCABE PJ, Barnason SA, Houfek J. 2011. Illness beliefs in patients with recurrent symptomatic atrial fibrillation. Pacing Clin Electrophysiol. 34:810–820.

McGraw KO, Wong SP. 1996. Forming inferences about some intraclass correlation coefficients. Psychol Methods. 1:30.

Millasseau SC, Ritter JM, Takazawa K, Chowienczyk PJ. 2006. Contour analysis of the photoplethysmographic pulse measured at the finger. J Hypertens. 24:1449–1456.

Mincic AM. 2015. Neuroanatomical correlates of negative emotionality-related traits: A systematic review and meta-analysis. Neuropsychologia. 77:97–118.

Mitra A, Snyder AZ, Blazey T, Raichle ME. 2015. Lag threads organize the brain's intrinsic activity. Proc Natl Acad Sci USA. 112:E2235–E2244.

Mizeva I, Di Maria C, Frick P, Podtaev S, Allen J. 2015. Quantifying the correlation between photoplethysmography and laser Doppler flowmetry microvascular low-frequency oscillations. J Biomed Opt. 20:037007–037007.

Monfredi O, Lyashkov AE, Johnsen A-B, Inada S, Schneider H, Wang R, Nirmalan M, Wisloff U, Maltsev VA, Lakatta EG. 2014. Biophysical characterization of the underappreciated and important relationship between heart rate variability and heart rate. Hypertension: Hypertensionaha. 114:03782.

Moore CI, Cao R. 2008. The hemo-neural hypothesis: on the role of blood flow in information processing. J Neurophysiol. 99: 2035–2047.

Müller LE, Schulz A, Andermann M, Gäbel A, Gescher DM, Spohn A, Herpertz SC, Bertsch K. 2015. Cortical representation of afferent bodily signals in borderline personality disorder: neural correlates and relationship to emotional dysregulation. JAMA Psychiatry. 72:1077–1086.

Murphy K, Birn RM, Bandettini PA. 2013. Resting-state fMRI confounds and cleanup. Neuroimage. 80:349–359.

Nardi AE, Valença AM, Mezzasalma MA, Levy SP, Lopes FL, Nascimento I, Freire RC, Veras AB, Zin WA. 2006. Comparison between hyperventilation and breath-holding in panic disorder: patients responsive and non-responsive to both tests. Psychiatry Res. 142:201–208.

Nikolaou F, Orphanidou C, Papakyriakou P, Murphy K, Wise R, Mitsis G. 2016. Spontaneous physiological variability modulates dynamic functional connectivity in resting-state functional magnetic resonance imaging. Phil Trans R Soc A. 374: 20150183.

Nikulin VV, Fedele T, Mehnert J, Lipp A, Noack C, Steinbrink J, Curio G. 2014. Monochromatic ultra-slow (~0.1 Hz) oscillations in the human electroencephalogram and their relation to hemodynamics. Neuroimage. 97:71–80.

Nitzan M, Turivnenko S, Milston A, Babchenko A, Mahler Y. 1996. Low-frequency variability in the blood volume and in the blood volume pulse measured by photoplethysmography. J Biomed Opt. 1:223–229.

Oppenheim AV, Schafer RW, Buck JR. 1999. Discrete-Time Signal Processing. Upper Saddle River, NJ: Prentice Hall.

Park H-D, Correia S, Ducorps A, Tallon-Baudry C. 2014. Spontaneous fluctuations in neural responses to heartbeats predict visual detection. Nat Neurosci. 17:612–618.

Park G, Thayer JF. 2014. From the heart to the mind: cardiac vagal tone modulates top-down and bottom-up visual perception and attention to emotional stimuli. Front Psychol. 5: 278.

Peterson EC, Wang Z, Britz G. 2011. Regulation of cerebral blood flow. Int J Vasc Med. 2011:1–8.

Pfeifer G, Garfinkel SN, van Praag CDG, Sahota K, Betka S, Critchley HD. 2017. Feedback from the heart: emotional learning and memory is controlled by cardiac cycle, interoceptive accuracy and personality. Biol Psychol. 126:19–29.

Phillips ME, Sachdev RN, Willhite DC, Shepherd GM. 2012. Respiration drives network activity and modulates synaptic and circuit processing of lateral inhibition in the olfactory bulb. J Neurosci. 32:85–98.

Pollatos O, Kirsch W, Schandry R. 2005. Brain structures involved in interoceptive awareness and cardioafferent signal processing: a dipole source localization study. Hum Brain Mapp. 26:54–64.

Power JD, Barnes KA, Snyder AZ, Schlaggar BL, Petersen SE. 2012. Spurious but systematic correlations in functional connectivity MRI networks arise from subject motion. Neuroimage. 59:2142–2154.

Pozuelo L. 2012. Fine-tuning a heart-brain connection anxiety in atrial fibrillation. Circ Heart Failure. 5:307–308.

Quas JA, Yim IS, Oberlander TF, Nordstokke D, Essex MJ, Armstrong JM, Bush N, Obradović J, Boyce WT. 2014. The symphonic structure of childhood stress reactivity: patterns of sympathetic, parasympathetic, and adrenocortical responses to psychological challenge. Dev Psychopathol. 26:963–982.

Revelle W, Wilt J. 2013. The general factor of personality: a general critique. J Res Pers. 47:493–504.

Reyes del Paso GA, Muñoz Ladrón de Guevara C, Montoro CI. 2015. Breath-holding during exhalation as a simple manipulation to reduce pain perception. Pain Medicine. 16:1835–1841.

Sadeghi MT, Namdar H, Vahedi S, Aslanabadi N, Ezzati D, Sadeghi B. 2013. Effects of emotional stimuli on cardiovascular responses in patients with essential hypertension based on brain/behavioral systems. J Cardiovasc Thoracic Res. 5: 167.

Salimi-Khorshidi G, Douaud G, Beckmann CF, Glasser MF, Griffanti L, Smith SM. 2014. Automatic denoising of functional MRI data: combining independent component analysis and hierarchical fusion of classifiers. Neuroimage. 90:449–468.

Samuels ER, Szabadi E. 2008. Functional neuroanatomy of the noradrenergic locus coeruleus: its roles in the regulation of arousal and autonomic function part ii: physiological and pharmacological manipulations and pathological alterations of locus coeruleus activity in humans. Curr Neuropharmacol. 6:254–285.

Schmukle SC, Egloff B, Burns LR. 2002. The relationship between positive and negative affect in the positive and negative affect schedule. J Res Pers. 36:463–475.

Schäfer A, Vagedes J. 2013. How accurate is pulse rate variability as an estimate of heart rate variability?: a review on studies comparing photoplethysmographic technology with an electrocardiogram. Int J Cardiol. 166:15–29.

Shelley KH. 2007. Photoplethysmography: beyond the calculation of arterial oxygen saturation and heart rate. Anesth Analg. 105:S31–S36.

Shmueli K, van Gelderen P, de Zwart JA, Horovitz SG, Fukunaga M, Jansma JM, Duyn JH. 2007. Low-frequency fluctuations in the cardiac rate as a source of variance in the resting-state fMRI BOLD signal. Neuroimage. 38:306–320.

Smith SM, Andersson J, Auerbach EJ, Beckmann CF, Bijsterbosch J, Douaud G, Duff E, Feinberg DA, Griffanti L, Harms MP, et al, the WUMHCPC. 2013. Resting-state fMRI in the Human Connectome Project. Neuroimage. 80:144–168.

Smith DJ, Escott-Price V, Davies G, Bailey MES, Colodro-Conde L, Ward J, Vedernikov A, Marioni R, Cullen B, Lyall D, et al. 2016. Genome-wide analysis of over 106[thinsp]000 individuals identifies 9 neuroticism-associated loci. Mol Psychiatry. 21(11): 1644.

Smith SM, Fox PT, Miller KL, Glahn DC, Fox PM, Mackay CE, Filippini N, Watkins KE, Toro R, Laird AR. 2009. Correspondence of the brain's functional architecture during activation and rest. Proc Natl Acad Sci USA. 106:13040–13045.

Stauss HM. 2003. Heart rate variability. Am J Physiol-Regul Integr Comp Physiol. 285:R927–R931.

Steinhubl SR, Wineinger NE, Patel S, Boeldt DL, Mackellar G, Porter V, Redmond JT, Muse ED, Nicholson L, Chopra D. 2015. Cardiovascular and nervous system changes during meditation. Front Hum Neurosci. 9:145.

Suls J, Martin R, David JP. 1998. Person-environment fit and its limits: Agreeableness, neuroticism, and emotional reactivity to interpersonal conflict. Pers Soc Psychol Bull. 24:88–98.

Taylor KS, Kucyi A, Millar PJ, Murai H, Kimmerly DS, Morris BL, Bradley TD, Floras JS. 2015. Association between resting-state brain functional connectivity and muscle sympathetic burst incidence. J Neurophysiol. 115:662–673.

Termenon M, Jaillard A, Delon-Martin C, Achard S. 2016. Reliability of graph analysis of resting state fMRI using test-retest dataset from the Human Connectome Project. Neuroimage. 142:172–187.

Thayer JF, Lane RD. 2000. A model of neurovisceral integration in emotion regulation and dysregulation. J Affect Disord. 61: 201–216.

Thayer JF, Lane RD. 2002. Perseverative thinking and health: neurovisceral concomitants. Psychol Health. 17:685–695.

Triggiani AI, Valenzano A, Del Percio C, Marzano N, Soricelli A, Petito A, Bellomo A, Başar E, Mundi C, Cibelli G. 2016. Resting state Rolandic mu rhythms are related to activity of sympathetic component of autonomic nervous system in healthy humans. Int J Psychophysiol. 103:79–87.

Turalska M, Latka M, Czosnyka M, Pierzchala K, West BJ. 2008. Generation of very low frequency cerebral blood flow fluctuations in humans. Acta Neurochira Suppl Springer. 102: 43–47.

Van Essen DC, Smith SM, Barch DM, Behrens TE, Yacoub E, Ugurbil K, Consortium W-MH. 2013. The WU-Minn human connectome project: an overview. Neuroimage. 80:62–79.

Van Essen DC, Ugurbil K, Auerbach E, Barch D, Behrens T, Bucholz R, Chang A, Chen L, Corbetta M, Curtiss SW. 2012. The Human Connectome Project: a data acquisition perspective. Neuroimage. 62:2222–2231.

Volkow ND, Tomasi D, Wang G-J, Fowler JS, Telang F, Goldstein RZ, Alia-Klein N, Woicik P, Wong C, Logan J. 2011. Positive emotionality is associated with baseline metabolism in orbitofrontal cortex and in regions of the default network. Mol Psychiatry. 16:818–825.

von Leupoldt A, Keil A, Chan P-YS, Bradley MM, Lang PJ, Davenport PW. 2010. Cortical sources of the respiratory-related evoked potential. Respir Physiol Neurobiol. 170: 198–201.

Wallin BG, Charkoudian N. 2007. Sympathetic neural control of integrated cardiovascular function: insights from measurement of human sympathetic nerve activity. Muscle Nerve. 36:595–614.

Wang YF, Long Z, Cui Q, Liu F, Jing XJ, Chen H, Guo XN, Yan JH, Chen HF. 2016. Low frequency steady-state brain responses modulate large scale functional networks in a frequency-specific means. Hum Brain Mapp. 37:381–394.

Welch P. 1967. The use of fast Fourier transform for the estimation of power spectra: A method based on time averaging over short, modified periodograms. IEEE Trans Audio Electroacoustics. 15:70–73.

Wiens S, Mezzacappa ES, Katkin ES. 2000. Heartbeat detection and the experience of emotions. Cogn Emot. 14:417–427.

Wilbert-Lampen U, Leistner D, Greven S, Pohl T, Sper S, Völker C, Güthlin D, Plasse A, Knez A, Küchenhoff H. 2008. Cardiovascular events during World Cup soccer. New England J Med. 358:475–483.

Winston JS, Rees G. 2014. Following your heart. Nat Neurosci. 17:482–483.

Wise RG, Ide K, Poulin MJ, Tracey I. 2004. Resting fluctuations in arterial carbon dioxide induce significant low frequency variations in BOLD signal. Neuroimage. 21:1652–1664.

Wittstein IS, Thiemann DR, Lima JA, Baughman KL, Schulman SP, Gerstenblith G, Wu KC, Rade JJ, Bivalacqua TJ, Champion HC. 2005. Neurohumoral features of myocardial stunning due to sudden emotional stress. New England J Med. 352:539–548.

Wong SW, Xue G, Bechara A. 2011. Integrating fMRI with psychophysiological measurements in the study of decision making. J Neurosci Psychol Econ. 4:85.

Xia Y, Yang L, Mao X, Zheng D, Liu C. 2017. Quantification of vascular function changes under different emotion states: a pilot study. Technol Health Care. 25:447–456.

Yuan H, Zotev V, Phillips R, Bodurka J. 2013. Correlated slow fluctuations in respiration, EEG, and BOLD fMRI. Neuroimage. 79: 81–93.

Zeng L-L, Wang D, Fox MD, Sabuncu M, Hu D, Ge M, Buckner RL, Liu H. 2014. Neurobiological basis of head motion in brain imaging. Proc Natl Acad Sci U S A. 111:6058–6062.

Zhang E, Liao P. 2015. Brain transient receptor potential channels and stroke. J Neurosci Res. 93:1165–1183.

Zimny ML, Schutte M, Dabezies E. 1986. Mechanoreceptors in the human anterior cruciate ligament. Anat Rec. 214: 204–209.